Geostatistical modeling of sound propagation: Principles and a field application experiment

Olivier Baume[a)]
Department of Environmental Sciences, Wageningen University, P.O. Box 47, 6700 AA Wageningen, The Netherlands

Benoit Gauvreau and Michel Bérengier
Section Acoustique Routière et Urbaine, Laboratoire Central des Ponts et Chaussées, Route de Bouaye, B.P. 4129, 44341 Bouguenais Cedex, France

Fabrice Junker
Département Analyses Mécaniques et Acoustique, EDF Recherche & Développement, 1 avenue du Général de Gaulle, 92141 Clamart Cedex, France

Hans Wackernagel and Jean-Paul Chilès
Centre de Géosciences/Géostatistique, Ecole des Mines de Paris, 35 rue Saint-Honoré, 77300 Fontainebleau, France

(Received 13 August 2008; revised 9 September 2009; accepted 14 September 2009)

The assessment of noise sources for environmental purposes requires reliable methods for mapping. Numerical models are well adapted for sophisticated simulations and sensitivity analyses; however, real-time mapping of large frequency bands must be based on fast and acceptable computations and honor *in situ* measurements. In this paper, a real-time mapping procedure of noise exposure is proposed. The procedure is based on geostatistical modeling of spatial variations and applied to a case study taken from an experimental campaign, where a point source was placed on a flat meadow. An analytical approximation of the acoustic field was first computed with the Embleton model. The difference between this approximation and the actual measurements ($L_{\mathrm{eq15\ min}}$ 1/3-octave bands samples from 19 microphones spread over the meadow) showed spatial structure, which has been modeled with a variogram. Finally, the geostatistical technique of kriging with external drift provided an optimal interpolation of the acoustic field data while encapsulating the first approximation from the Embleton model. Systematic geostatistical inference and real-time mapping with the proposed procedure can be envisaged in simple cases.
 [DOI: 10.1121/1.3243301]

PACS number(s): 43.28.Tc, 43.28.Lv, 43.28.En [KVH] Pages: 2894–2904

I. INTRODUCTION

Real-time mapping of sound exposure in semi-open areas has never been attempted although it is of high interest for practical purposes. The assessment of sound exposure in semi-open areas is a difficult task. In semi-open areas, micrometeorology and ground properties have a major influence on sound propagation. Additionally micrometeorology and ground properties change continuously in time and space. Therefore, with the use of experimental data and a limited number of measurement locations in space, propagation conditions can only be known approximately. Prediction models need to take advantage of deterministic models with a growing complexity of the influence of physical parameters: ground effect,[1–3] mean refraction indices, and knowledge on the turbulence structure.[4,5] The notion of randomness already exists in numerical propagation models: for example, the scattering effect of turbulence is considered through the inclusion of physical randomness.[6,7]

In a prediction context, where generally time is hardly involved, highly complex models require a large amount of input data.[8,9] For the purpose of real-time mapping, the use of such models is unrealistic. Rather, a trade-off between the loss of complexity in the physical model and a possible estimation of the embedded error must be found to obtain, in the long run, an appropriate assessment method.

Séchet showed in a previous study[10] that partial information on mean refraction conditions and on the turbulence structure may lead to a loose statistical relationship between micrometeorological measurements and sound level records. He also concluded that, for the purpose of assessment, sound fields in semi-open areas should be modeled as random fields. The spatial structure of the sound field is statistically much easier to evaluate, though, when setting the integration time step of acoustical time series at 15 min.[10,11] At this time scale, mean vertical sound celerity gradients are representative of mean propagation conditions.

The objective of our research was to develop a well-adapted method to assess and map the acoustical impact of sound sources in semi-open areas. We intended to work first on a simplified case study of noise pollution where the

[a)]Author to whom correspondence should be addressed. Electronic mail: obaume@hotmail.com

source characteristics are known and constant in time, a case where the ground is flat and has slowly varying acoustical properties, and still a case where micrometeorological conditions are measured as well. We wanted to demonstrate that it is practically feasible to model the sound pressure as a random function and, finally, we aimed at evaluating potential applications.

In semi-open areas, the complex influence of micrometeorological conditions and impedance conditions requires to combine both physical modeling and statistical knowledge.[8,9] Physical models provide the main spatial characteristics of the sound field, and statistical methods introduce an uncertainty estimation of the final assessment. In our context, computation time was also considered to be an important factor for practical applications. Hence we considered simplified physical models to be of interest. The prediction provided by a simplified physical model is an approximation of reality. The actual difference between a deterministic approximation of reality and measurements is then viewed as the outcome of a random process, and the spatial structure of such a random process may be characterized by means of statistical inference.

Geostatistics emerged as a collection of statistical techniques for spatial data in a mining industry context.[12] Matheron[13] developed the theoretical basis for its use (see Ref. 14 for a more complete historical review). Applications of geostatistics in environmental issues are numerous. For instance, geostatistical modeling proved efficient in assessing air pollution.[15] In particular, the interest of geostatistics is when the mean underlying physical process is known and can be modeled. This is the case in sound propagation. One issue remains in the choice of the acoustical model to be included. In a method that combines a physical model with statistical tools, it is crucial to find a good trade-off between simplicity, computation time, and compatibility with geostatistical assumptions.

In this article, we aim at introducing geostatistical principles and consider opportunities to infer a geostatistical model for automatic mapping in a simple context. The choice is oriented toward a physical model that does not include micrometeorology in the present case study: the Embleton model.[3] Then, we show how geostatistics can handle differences between a simple physical model such as the Embleton model and measurements which vary under the influence of wind and temperature.

The remainder of the article is structured as follows. In Sec. II, we introduce the principles of geostatistics with an emphasis on its main analysis tool called the variogram and its use in statistical interpolation. In Sec. III, we present the case study, a simple example of sound propagation from a point source in a flat meadow field. In Sec. IV, we describe the different computational steps of the geostatistical study. The computational steps include the choice of an adequate physical model as a first guess of the sound field, the analysis of the fluctuations between this guess and the measurements ($L_{\mathrm{eq15\ min}}$), and finally an interpolation of the data taking account of the guess field. The illustration concerns mid-frequency propagation (1/3-octave band centered on 1 kHz) where the sound field is more erratic than at lower frequency and has an important impact on the environment. Results are interpreted and discussed in Sec. V.

II. INTRODUCTION TO GEOSTATISTICS

The main fact that leads to the application of geostatistics for mapping is the observation of spatial auto-correlation in the studied phenomenon: the closer two measurement locations, the more likely their acoustic levels will be correlated. Geostatistics developed a whole theoretical framework for optimizing mapping in such a situation. We present in this section the basis on which sound propagation can be modeled with geostatistical tools.

A. The variogram

The spatial and temporal uncertainties in micrometeorological conditions, ground acoustical properties, and sound propagation are a major challenge in assessing the acoustic exposure in a spatial domain. Geostatistical methods are designed for solving estimation problems based on the spatial data and numerical model output. Geostatistical methods rely on a probabilistic framework that is appropriate for describing phenomena in space and time.

The starting point is a regionalized variable $p(\mathbf{x})$ describing the value of the acoustic pressure field at location $\mathbf{x}$ in a spatial domain $\mathcal{D}$. In the present paper, $p(\mathbf{x})$ will be expressed as the sound pressure relative to a reference pressure measured or calculated 10 m from the sound source. This relative sound pressure is expressed in decibels (dB) for each 1/3-octave band. In addition, we define the spatial domain $\mathcal{D}$ of geostatistical study as a two-dimensional (2D) horizontal domain so that $\mathbf{x}=\{x_1,x_2\}\in\Re^2$.

Reality $p(\mathbf{x})$, from which data are sampled, is considered as a realization of a random function, by which we mean a collection of random variables $\{P(\mathbf{x}),\mathbf{x}\in\mathcal{D}\}$. To ease notation, the curly brackets are dropped and the random function is simply written $P(\mathbf{x})$.

A convenient assumption is to consider that the variance of the difference $P(\mathbf{x})-P(\mathbf{x}')$ for any two locations $\mathbf{x}$ and $\mathbf{x}'$ is translation invariant, $\mathrm{var}(P(\mathbf{x})-P(\mathbf{x}'))=2\gamma(\mathbf{h})$, i.e., the variance only depends on the vector $\mathbf{h}=\mathbf{x}-\mathbf{x}'$ and not on the position of the vector in $\mathcal{D}$. If we further assume that the expectation of the increments is zero, $E[P(\mathbf{x})-P(\mathbf{x}')]=0$, we obtain the expression

$$\gamma(\mathbf{h})=\tfrac{1}{2}E[(P(\mathbf{x})-P(\mathbf{x}'))^2], \tag{1}$$

which is called the variogram. The above assumption is called *intrinsic stationarity*.

B. Kriging

The problem at hand is to attempt the reconstruction of a phenomenon over a continuous spatial domain based on the measured values, only available at a limited number of sampling locations. The procedure known as *kriging* [after D. G. Krige who proposed it in 1951 (Ref. 12)] consists in searching for the linear estimator that bears the smallest estimation variance. This leads to a system of linear equations (kriging

equations) whose solution provides the weights corresponding to a minimum estimation variance (kriging variance[16,17]). There are close links between splines and kriging despite differences in their practical implementation.[16]

The starting point for estimating P at an unsampled location $\mathbf{x}_0$ is a linear estimator P^* assigning weights w_α to data at locations $\mathbf{x}_\alpha$, $\alpha=1,\ldots,n$,

$$P^*(\mathbf{x}_0)=\sum_{\alpha=1}^{n} w_\alpha P(\mathbf{x}_\alpha). \tag{2}$$

Second, two assumptions will lead to express the statistical moments of the estimator through a linear estimation of weights w_α. First assumption, the estimator is unbiased at all locations of the study domain $\mathcal{D}$, hence writing the particular case at measurement locations

$$P^*(\mathbf{x}_\alpha)=P(\mathbf{x}_\alpha)=\sum_{\alpha=1}^{n} w_\alpha P(\mathbf{x}_\alpha), \quad \alpha=1,\ldots,n. \tag{3}$$

The latter relationship is independently built on the value of P. Thus, at any location $\mathbf{x}_0$ of domain $\mathcal{D}$, the weights w_α are solution of

$$1=\sum_{\alpha=1}^{n} w_\alpha. \tag{4}$$

Second assumption, the intrinsic stationarity [stationarity of the second moment of $P(\mathbf{x})$] allows to use the definition of the variogram $\gamma(\mathbf{x})$ given in Eq. (1).

If the statistical mean of $P(\mathbf{x})$ (in the sense of a Gaussian distribution) is further assumed to be constant over $\mathcal{D}$, the most commonly used estimator is called *ordinary kriging*. In the case of ordinary kriging, weights w_α are solution of the linear system

$$\begin{cases} \displaystyle\sum_{\beta=1}^{n} w_\beta \gamma(\mathbf{x}_\beta-\mathbf{x}_\alpha)+\mu=\gamma(\mathbf{x}_0-\mathbf{x}_\alpha), & \alpha=1,\ldots,n, \\ \displaystyle\sum_{\alpha=1}^{n} w_\alpha=1. \end{cases} \tag{5}$$

In its left-hand side, the system incorporates the variogram values $\gamma(\mathbf{x}_\beta-\mathbf{x}_\alpha)$ between all sample point pairs, while in its right-hand side, we find the variogram values $\gamma(\mathbf{x}_0-\mathbf{x}_\alpha)$ between the estimation location and each sampling location. The second equation that ensures unbiasedness of the estimator explains the presence of an additional variable (the Lagrange parameter μ), which brings an extra degree of freedom in the linear system.

The expression of the minimum estimation variance in case of ordinary kriging is

$$\sigma^2_{\mathrm{OK}}(\mathbf{x}_0)=\sum_{\alpha=1}^{n} w_\alpha \gamma(\mathbf{x}_0-\mathbf{x}_\alpha)+\mu. \tag{6}$$

C. Kriging with external drift

The assumption of intrinsic stationarity may not be suitable if there is a systematic trend in the spatial domain. Such a systematic change can often be described by a numerical model implementing physical equations. The output $\rho(\mathbf{x})$ from such a mechanistic model provides a tentative description of reality $P(\mathbf{x})$ that can be used as another piece of information in addition to measurement values $P(\mathbf{x}_\alpha)$. In such a situation, we will assume that the random function is decomposed into two components

$$P(\mathbf{x})=m(\mathbf{x})+\epsilon(\mathbf{x}) \tag{7}$$

where $\epsilon(\mathbf{x})$ is a zero-mean intrinsic random function called the residuals and $m(\mathbf{x})$ is a deterministic drift. The objective is to use the physical model output $\rho(\mathbf{x})$ in order to obtain a physically sound estimate of the mean $m(\mathbf{x})$, while $\epsilon(\mathbf{x})$ bears the second moment characteristics of $P(\mathbf{x})$—in the sense of Gaussian distribution the variance is a sufficient descriptor of a statistical distribution.

To better assess the trend (on the basis of measurement values), $m(\mathbf{x})$ is assumed to be linearly related to the model output and to spatial coordinates $\mathbf{x}=(x_1,x_2)$ in a 2D horizontal domain:

$$E[P(\mathbf{x})]=m(\mathbf{x})=a+b\rho(\mathbf{x})+c_1x_1+c_2x_2. \tag{8}$$

If we constrain the estimator (2) to interpolate the drift component without error whatever the coefficients a and b, we obtain the equations of kriging with external drift:

$$\begin{cases} \displaystyle\sum_{\beta=1}^{n} w_\beta \gamma(\mathbf{x}_\alpha-\mathbf{x}_\beta)+\mu_1+\mu_2\rho(\mathbf{x}_\alpha)+\mu_3x_{1\beta}+\mu_4x_{2\beta} \\ \qquad =\gamma(\mathbf{x}_\alpha-\mathbf{x}_0), \quad \alpha=1,\ldots,n, \\ \displaystyle\sum_{\beta=1}^{n} w_\beta=1, \\ \displaystyle\sum_{\beta=1}^{n} w_\beta\rho(\mathbf{x}_\beta)=\rho(\mathbf{x}_0), \\ \displaystyle\sum_{\beta=1}^{n} w_\beta x_{1\beta}=x_{10}, \\ \displaystyle\sum_{\beta=1}^{n} w_\beta x_{2\beta}=x_{20}. \end{cases} \tag{9}$$

It should be noted that the coefficients a, b, c_1, and c_2 of the external drift do not appear in the system as they are estimated implicitly. An explicit estimation of these coefficients is possible, using a different set of equations[17,18] (see Sec. IV B).

D. Variogram model

An empirical variogram $\hat{\gamma}(h)$ can be computed from the data using the formula

$$\hat{\gamma}(h)=\frac{1}{2N(h)}\sum_{|\mathbf{x}_\alpha-\mathbf{x}_\beta|\approx h}(P(\mathbf{x}_\alpha)-P(\mathbf{x}_\beta))^2, \tag{10}$$

where $N(h)$ is the number of pairs of measurements.

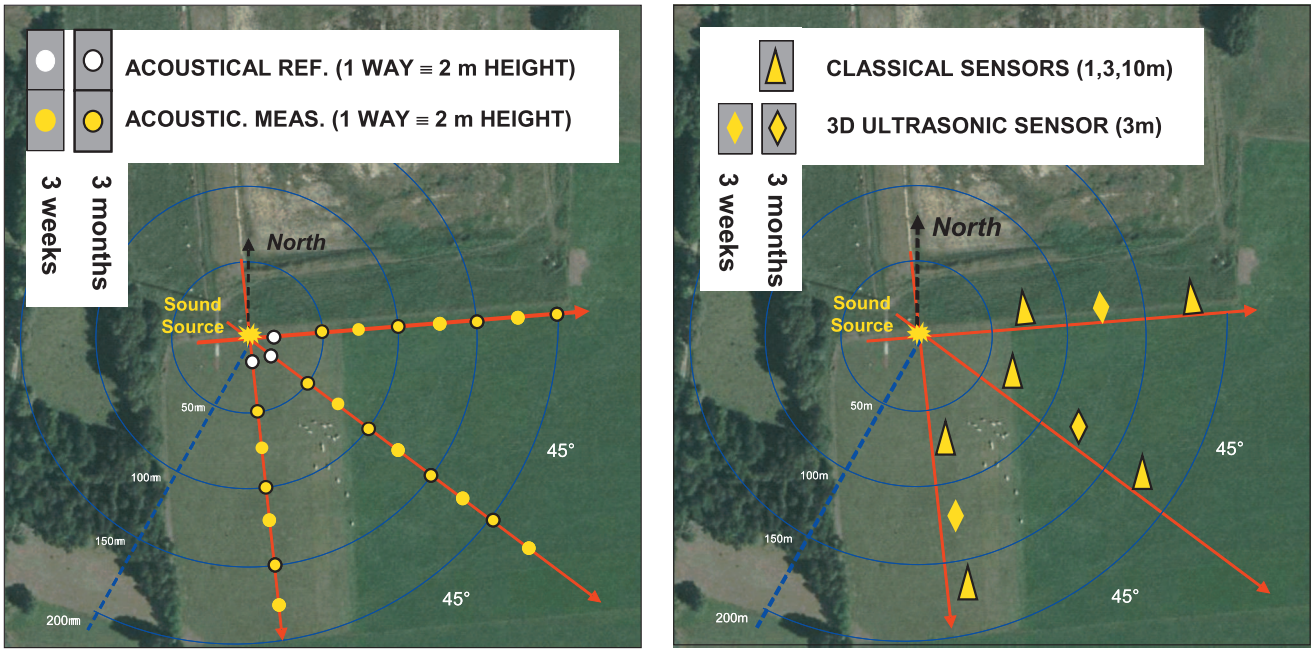

(a) (b)

FIG. 1. Experimental setup of Lannemezan campaign in 2005: the sound source and the microphones are placed 2 m above the flat ground: (a) microphones and (b) micrometerological towers.

In the case of ordinary kriging, a theoretical variogram is fitted to the empirical variogram of $P(\mathbf{x})$, while in the case of kriging with external drift, the theoretical variogram is adjusted to the empirical variogram of the residuals $\epsilon(\mathbf{x})$. A variogram is a conditionally negative definite function and several classes of variogram models are available, allowing to comply with different behaviors of the empirical variogram and different physical contexts.

III. THE CASE STUDY

Sound propagation is a non-stationary process in space and time. Geometrical spreading of wave fronts yields a decrease in sound energy with the distance from the source. The first case study of geostatistical inference needs to fulfill two main criteria:

- to be a well-known example that is easily approximated with a simple analytical model and
- to have a high sensitivity with respect to micrometeorology and ground effects.

Point sources are easier to model than extended sources (e.g. lineic sound sources) and their advantage is that they bear the highest variability of the sound field in space, especially due to the wind direction changes. Thus installing a point source above a flat meadow field seemed a reasonable and well-adapted case study for a first geostatistical work on outdoor sound propagation.

A. The experimental setup and validation of the measurements

We tuned a Bruel & Kjaer source, type 4292 to deliver a 118 dB(A) pink noise during the experiment, its emission power being controlled in a continuous manner with reference measurements 10 m away [see Fig. 1(a)]. The source was placed 2 m above a flat meadow located on a plateau in the area of the Pyrénées mountains (Lannemezan, France). The experiment lasted 3 months on a continuous basis (from early June to late August, 2005). A spatial mean of acoustical properties of the ground was estimated from 13 locations. Measurements of impedance were carried out almost every day during the first 3 weeks (in June) and once a week in the last part of the campaign. One additional impedance monitoring point was placed close to the source (one measurement each 4 h during 3 months).

Sound pressure levels were recorded with 19 microphones during the period of June. Measurements were spatially sampled following three propagation axes which draw a 90° angle around the source [Fig. 1(a)]. We chose this design in order to record acoustical levels under various propagation conditions. The microphones were placed 2 m above the ground. $L_{\mathrm{eq1\ s}}$ samples have been stored for 1/3-octave bands centered on frequencies from 50 Hz to 4 kHz. Propagation conditions were recorded with micrometeorological towers equipped with classical sensors (1 Hz sampling frequency devices as vane anemometers, weather vanes, and ventilated temperature probes) and ultrasonic sensors (20 Hz sampling frequency). Sensors were located as in Fig. 1(b). Micrometeorological data were not included in the geostatistical model but we relied on them for physical interpretation of the results.

A strict validation process was designed and carried out in order to leave out any suspicious sample from the final acoustical and micrometeorological databases. Rainy or too windy conditions (wind speed >5 m/s) were excluded. We selected turbulence data in the validity domain of the Monin–Obukhov similarity theory[19] ($-2<z/L_{\mathrm{MO}}<1$, where z is the height and L_{MO} the Monin–Obukhov length). More-

over Monin–Obukhov theory has been used to derive vertical sound speed profiles from vertical wind and temperature profiles using universal functions with Businger–Dyer empirical parameters.[20] Those experimental (turbulent) data have been cross-correlated with meteo-towers (classical) profiles, in order to verify (or not) the range dependence of the sound speed profiles along each propagation axis during each 15 min sample.

We also filtered out extraneous acoustical events (trains passing by in the valley, road traffic close by, insects noise on the meadow during summertime). The automatic procedure for validation included the use of a characteristic calibration spectrum (envelop spectrum based on the overall temporal mean) at each measurement location. More details on the data validation procedure for this experimental campaign can be found in Ref. 21.

B. The acoustic samples and ground measurements

Although 1-s samples were available from the database ($L_{\mathrm{eq1\ s}}$), the most easily interpretable time series has a 15-min integration interval as mentioned in the Introduction. Thus an integration of acoustical samples was carried out ($L_{\mathrm{eq15\ min}}$). After the validation process, the database was lacking spatial information for a number of time steps. Yet the geostatistical study based on the modeling of spatial autocorrelation should be done with a maximum number of spatial samples.

After the validation process described in Sec. III A, we selected a whole day of acoustical data: the 22 June 2005. Micrometeorological conditions changed substantially from clear night conditions to sunny morning and sunny afternoon conditions of early summer (temperature vertical gradient from positive to negative values), and back to clear night conditions during the evening. We based the case study on two typical 1/3-octave bands for road traffic or industrial noise outdoor propagation: a characteristic band for low frequencies (100 Hz) and a characteristic band for mid-frequencies (1 kHz). Higher 1/3-octave bands could have been selected and included in the sequel. However, considering our sound source, signal to noise ratio is poor for high frequencies (1/3-octave bands superior to 2 kHz) and for long distances (receivers farther than 100 m). After the validation procedure, the experimental database is reduced for those 1/3-octave bands and receiver locations. Thus only a few 15-min samples were validated at high frequencies for this kriging procedure.

We also selected the most representative ground properties values (for a more detailed study on ground impedance measurements for this campaign see Ref. 22). These correspond to the impedance measurements carried out the 20 June 2005. No major precipitation event happened to modify ground properties of the meadow between the 20th and the 22nd in June. Finally, in order to build the final acoustical database for the study, measured acoustic levels (up to 200 m from the source) were expressed in sound pressure levels (SPLs) relative to the reference microphone of the corresponding propagation axis. This allowed us to minimize the effect of spatial directivity and temporal fluctuations (amplitude and spectrum) of the sound source.

Sections IV and V present the application of kriging modeling to this case study. A detailed description of the method is given in Sec. IV for the 1 kHz 1/3-octave band sample ($L_{\mathrm{eq15\ min}}$), recorded between 23:45 and 24:00, on 22 June 2005. The 1 kHz database is more critical than the 100 Hz example because the spatial structure is more irregular (interference patterns due the ground reflection) and more fluctuating as well. Same steps in the modeling process are followed at 100 Hz. In Sec. V, results and discussion also include the low frequency case.

IV. MODELING THE ACOUSTIC FIELD WITH KRIGING

The non-stationarity context of the case study (in the spatial sense) suggests the use of kriging with external drift. The statistical distribution of the measurements for one time sample (19 $L_{\mathrm{eq15\ min}}$ for the SPL) cannot show the Gaussian distribution characteristics of a stationary process because SPL measurements have various positions in terms of source-receiver distance. The interpolation procedure follows five steps.

- Step 1: A description of the deterministic part of the acoustic field is generated using the Embleton propagation model and the Delany and Bazley ground model. A mean value of ground properties over the study domain is used.
- Step 2: The Embleton model is fitted to the measurements using a least squares procedure. This step leads to a preliminary estimation of the drift (the deterministic part of the geostatistical model).
- Step 3: The difference (called residuals) between measurements and the fitted Embleton model (both expressed in SPL relative to the reference microphone located 10 m from the source and 2 m above the ground) is computed. The variogram of the residuals is computed as well.
- Step 4: A variogram model is fitted to the sample variogram of the residuals.
- Step 5: Kriging is used for mapping.

The first four steps can be seen as the inference steps; the model is being built up and its parameters are estimated. The last step is the interpolation step using the inferred model.

A. Step 1: Computation of the first-order physical model

We computed a first-order approximation of the acoustic attenuation (SPL relative to a reference microphone) with the Embleton model.[3] The acoustic attenuation is computed relatively to the reference microphone 10 m away from the source located on the same propagation direction. The general form of the acoustic pressure above a porous half-space in a 2D horizontal domain at location $\mathbf{x}=(x_1,x_2)$ is given by

$$p_E(\mathbf{x}) = \frac{A_d}{r_d(\mathbf{x})}\exp(ik_d r_d(\mathbf{x})) + Q\frac{A_r}{r_r(\mathbf{x})}\exp(ik_r r_r(\mathbf{x})). \quad (11)$$

r_d is the direct travel distance from the source [located at $\mathbf{x}=(0,0)$] to the receiver location $\mathbf{x}=(x_1,x_2)$. r_r is the travel distance of the reflected wave. A_d and A_r are the amplitudes of the direct and reflected waves, respectively, and k_d and k_r are the associated wave numbers. To compute the drift, we assume no turbulence on the wave path. Hence we have $A_d=A_r$ and $k_d=k_r=k_0$, where k_0 is the wave number in the air. Direct and reflected sound ray distances are, respectively,

$$r_d=\sqrt{\mathbf{x}^2+|h_S-h_R|^2},$$

$$r_r=\sqrt{\mathbf{x}^2+(h_S+h_R)^2}, \tag{12}$$

where h_S and h_R are the source and receiver heights. In the specific case of a study in a 2D horizontal plane, source and receiver heights are equal, hence simplifying the previous to

$$r_d=|\mathbf{x}|,$$

$$r_r=\sqrt{\mathbf{x}^2+4h_S^2}. \tag{13}$$

Q is the complex form of the spherical reflection coefficient of the porous ground.[23] In the considered case (propagation distance greater than the wave length), the expression of Q can be approximated by

$$Q=R_p+(1-R_p)F(w), \tag{14}$$

where the plane wave reflection coefficient R_p is

$$R_p=\frac{\sin\phi_i-\mathcal{Z}_0/\mathcal{Z}_G}{\sin\phi_i+\mathcal{Z}_0/\mathcal{Z}_G} \tag{15}$$

and

$$F(w)=2i\sqrt{w}e^{-w}\int_{-i\sqrt{w}}^{\infty}e^{-u^2}du. \tag{16}$$

ϕ_i is the incidence angle with the ground, $\mathcal{Z}_0$ the air impedance, and $\mathcal{Z}_G$ the ground impedance. The numerical distance w reads

$$w=\frac{2ik_0r_r}{(1-R_p)^2\cos^2\phi_i}(\mathcal{Z}_0/\mathcal{Z}_G)^2\left(1-\frac{k_0^2}{k^2}\cos^2\phi_i\right), \tag{17}$$

where k the characteristic wave number of the ground.

Through the numerical distance w and the reflection coefficient R_p, the expression of the field is dependent on the frequency and the ratio $\mathcal{Z}_0/\mathcal{Z}_G$. The computation for 1/3-octave bands is made using several calculations (from 1 to 7 monochromatic calculations for each 1/3-octave band[24]) to avoid local interference patterns. From the impedance measurements, we took into account a spatial average, whose value slowly fluctuates with time.[22] The computation consisted in giving a map of the relative SPL levels 2 m above the ground, following the height of the source and microphones.

Impedance of the ground is an input variable of the Embleton model. In practice, the impedance is assessed through a ground model that defines a relationship between the impedance and other parameters that are fitted with the actual measurements. In our case study, we computed the impedance with the Delany and Bazley phenomenological model.[1] We applied a two-parameter fitting procedure. The first parameter is the phenomenological parameter of the Delany and Bazley model: the specific airflow resistivity σ_G. The second parameter is the layer thickness e, assuming a perfectly reflective surface above e.[25]

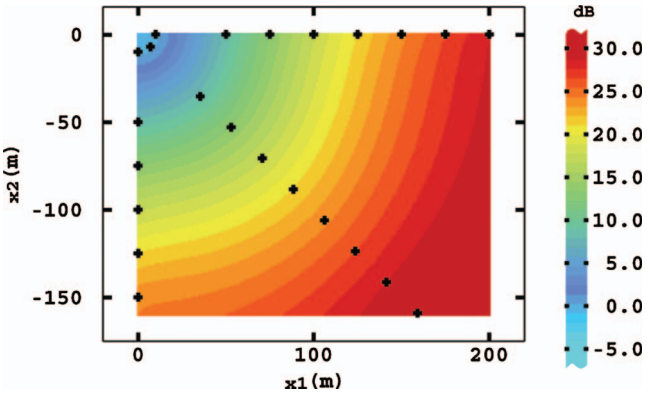

FIG. 2. Computation of SPL rel. to ref. microphone ($L_{eq15\ min}$) using the Embleton model at 1 kHz with mean ground properties: $\sigma_G=151$ kN s m^{-4} and $e=0.02$ m. Prediction height is 2 m above ground. Reference level is taken 10 m from the source and 2 m above ground.

The fitting procedure focused on the frequency range from 100 Hz to 1.5 kHz, leading to the following spatial average values for 20 June 2005:

$$\sigma_G=151\ \text{kN sm}^{-4},$$

$$e=0.02\ \text{m}.$$

Figure 2 displays a map of the SPL values using the Embleton model for the 1 kHz 1/3-octave band. It shows an isotropic propagation around the omni-directional source located in the upper left corner. Interference patterns are barely noticeable for this frequency, even close to the reference measurements mainly because of a coarse grid definition (2×2 m^2).

B. Step 2: Estimation of the trend

The Embleton model does not include micrometeorological conditions. The temperature field can lower or raise SPL values, in an isotropic manner, around the source, whereas the wind field has a vectorial effect. A way to make the Embleton predictions p_E statistically sensitive to micrometeorological conditions is to apply an additive factor a and a multiplicative factor b. In addition, in order to mimic more specifically the influence of wind conditions, a linear combination of the spatial coordinates $c_1\ x_1+c_2\ x_2$ can be added as well. The coefficients a, b, c_1, and c_2 are obtained through a regression procedure. Hence, we arrive to an external drift model of the form

$$P(\mathbf{x})=a+bp_E(\mathbf{x})+c_1x_1+c_2x_2+\varepsilon(\mathbf{x}). \tag{18}$$

P represents the statistical distribution of the acoustic field at any location $\mathbf{x}$, and $\varepsilon(\mathbf{x})$ represents a zero-mean random function associated to P. In a kriging procedure $\varepsilon(\mathbf{x})$ is assumed to be intrinsically stationary.

The regression procedure (to estimate the coefficients a, b, c_1 and c_2) uses two types of data: the computed Embleton model (from step 1) and measured acoustical data. The Em-

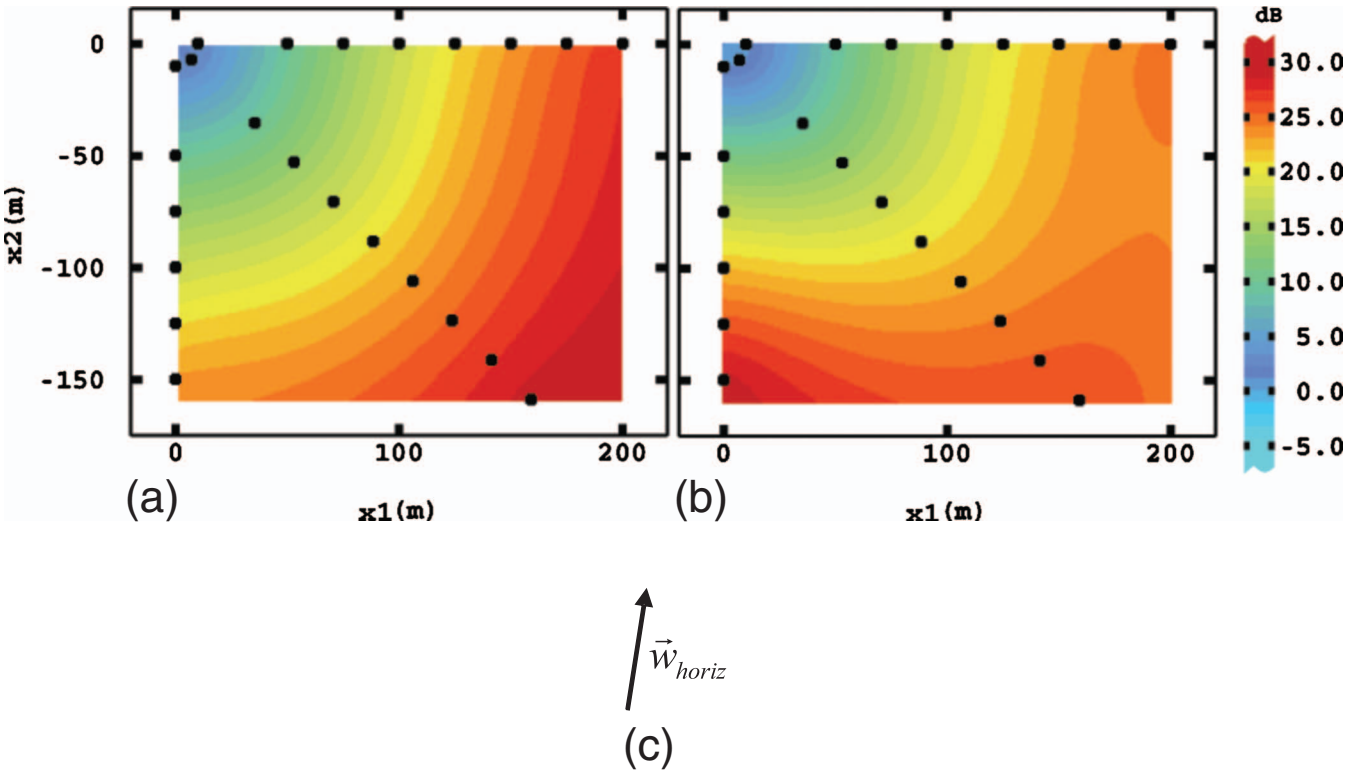

FIG. 3. Lannemezan campaign 22 June 2005 between 23:45 LST and 24:00 LST: fit of Embleton model at 1 kHz (SPL rel. to ref. microphone, $L_{\text{eq15 min}}$): (a) without linear drift and (b) including a linear drift. (c) Direction of mean horizontal wind speed. Prediction height is 2 m above ground.

bleton model is computed 2 m above the ground in terms of SPL relative to a reference level located 10 m from the source ($L_{\text{eq15 min}}$ for each 1/3-octave band, in dB). In the case of measurements, the reference level is taken from the microphone located 10 m from the source and 2 m above the ground on each propagation line (see the experiment protocol in Fig. 1).

Ordinary least squares is a classical method to estimate regression coefficients. At measurement locations, the mathematical expectation of P equals the measurement value. Hence, writing the mathematical expectation of P using Eq. (8) and applying the relationship at n measurement locations lead to

$$\begin{pmatrix} p(\mathbf{x}_1) \\ \vdots \\ p(\mathbf{x}_n) \end{pmatrix} = \begin{pmatrix} p(x_{11},x_{12}) \\ \vdots \\ p(x_{n1},x_{n2}) \end{pmatrix} = \begin{pmatrix} 1 & p_E(x_{11},x_{12}) & x_{11} & x_{12} \\ \vdots & \vdots & \vdots & \vdots \\ 1 & p_E(x_{n1},x_{n2}) & x_{n1} & x_{n2} \end{pmatrix} \begin{pmatrix} a \\ b \\ c_1 \\ c_2 \end{pmatrix}, \tag{19}$$

whose matrix form is

$$p = \mathbf{X}d. \tag{20}$$

Applying the least squares formalism leads to the estimate $\hat{d}$ of the regression coefficients:

$$\hat{d} = (\mathbf{X}'\mathbf{X})^{-1}\mathbf{X}'p. \tag{21}$$

In practice, the linear trend $c_1x_1+c_2x_2$ adds some flexibility in case of an anisotropic behavior of the acoustic field. We also checked the introduction of a quadratic component, but this proved to be irrelevant. In the sequel, we will only compare modeling with and without a linear component in the drift. These estimated drift maps are presented in Fig. 3. Figure 3(c) indicates the direction of the mean horizontal wind speed between 23:45 LST and 24:00 LST.

C. Step 3: Analysis of the variogram of the residuals

The empirical variogram of the residuals ε measures the part of the variability of the studied phenomenon that is not explained by the drift. A high explanatory power of the drift is associated with a low level (or sill) of the variogram of the residuals. Another important characteristic of the variogram is its correlation length (known as the range): namely, the distance at which the variogram reaches its sill. When computing the empirical variogram, one has to carefully choose the distance classes h_d. We tried various distance classes and finally retained classes of 15 m. Figure 4 presents the sample variogram of the residuals when the drift model does not include a linear trend (left plot) or includes a linear trend (right plot). The present case study at 1 kHz shows a clear difference (decreasing of the sill by a factor of 4) when including the linear drift into the drift model. The range then drops substantially from 120 to 90 m.

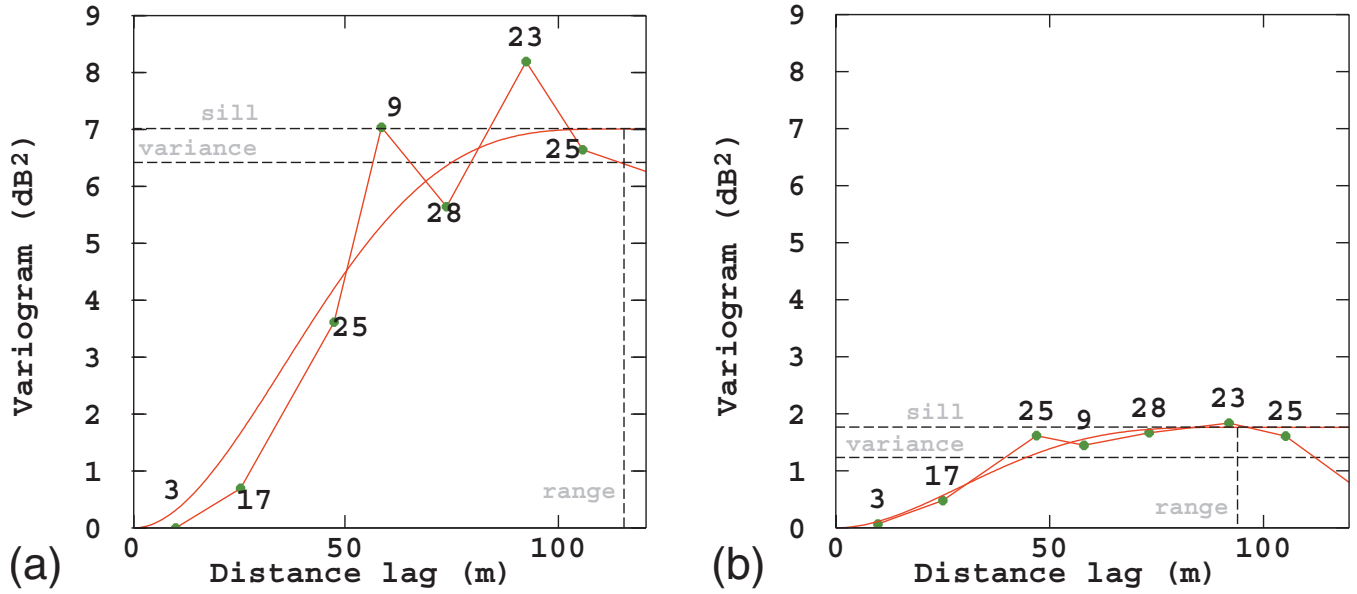

FIG. 4. Lannemezan campaign 22 June 2005 between 23:45 LST and 24:00 LST: empirical variogram of the residuals and associated model at 1 kHz (a) without linear drift and (b) including a linear drift. The horizontal dashed line shows the variance of the residuals. The vertical dashed line indicates the range of the variogram. The zero value at the origin shows that the process is spatially continuous, its parabolic behavior at short distances that it is even differentiable. Distance lag on the x coordinate axes means distance between measurements.

D. Step 4: Variogram fitting

Figure 4 presents the variograms of the residuals (computed from relative sound pressure levels) for both drift models for the 1 kHz data. The usefulness of a linear component in the drift is obvious, because it decreases the variance of the residuals (represented by a horizontal dashed line) as well as the variogram by a factor of 5. Both variograms present no discontinuity at the origin, which means that data do not seem to be affected by measurement errors. Both variograms show a parabolic behavior at short distances, which is the expression of a spatial continuity and differentiability of the acoustic field, which is consistent with physical intuition. They reach a sill at a distance of about 100 m (shorter when a linear component is included in the drift). That distance, called the range, measures the correlation length of the random part of the phenomenon. Kriging makes use of a theoretical variogram model that we have to fit to the sample variogram of the residuals. A great variety of theoretical models exist in the literature, but since we are interested in models with a parabolic behavior at the origin, we only checked the Gaussian model and the cubic model. The latter appeared as the most appropriate. Its expression is

$$\gamma(h) = \begin{cases} v\left(7\frac{h^2}{r^2} - 35/4\frac{h^3}{r^3} + 7/2\frac{h^5}{r^5} - 3/4\frac{h^7}{r^7}\right) & \text{for } h < r \\ v & \text{for } h \geq r, \end{cases} \tag{22}$$

where h is the spatial separation—also called lag—between two locations in meters, r is the range of the variogram (in meters), and v the sill of the variogram (in dB^2). The range and sill of all sample variograms were fitted manually by eye-fit. For eye-fitting, the three most important features are the value at lag 0 (the nugget effect), the range, and the total sill of the sample variogram. Depending on the geostatistical software, the fitting procedure may be more or less flexible depending on the interactive interface of the software. For an automatic process of kriging, automatic procedures also exist,[16] using maximum likelihood methods for instance.

E. Step 5: Prediction

Prediction was achieved by the application of kriging formulas (prediction and prediction error) at any location on the prediction grid. The prediction grid had a 2-m sized discrete mesh (7500 interpolation points). The kriging weights w_α were computed from the system of equations (9). Figure 5 depicts kriging results with both external drift models. Top graphs are the interpolation results. Bottom graphs are the kriging standard-deviation maps. Prediction locations closer to the measurement locations obtain a lower standard deviation value (becoming zero at the measurement locations as exactness is by design a property of the kriging predictor—see Sec. II).

V. RESULTS AND DISCUSSION

The above procedure was repeated for each 15-min validated sample ($L_{\text{eq15 min}}$) during the whole day of 22 June 2005 for 100 Hz and 1 kHz 1/3-octave bands. At both frequency bands, the method worked well. All variograms showed a parabolic behavior at the origin, indicating differentiability of the sound field even at mid-frequency (see Fig. 4). They were easily fitted with a cubic variogram model (with varying range and sill). At 100 Hz, the sill of the variogram is ten times lower than at 1 kHz. Such a difference indicates a better approximation of the field at low frequency when the external drift includes the Embleton model. At low frequency, spatial interferences between direct field and reflected field have larger structures in a semi-open area.

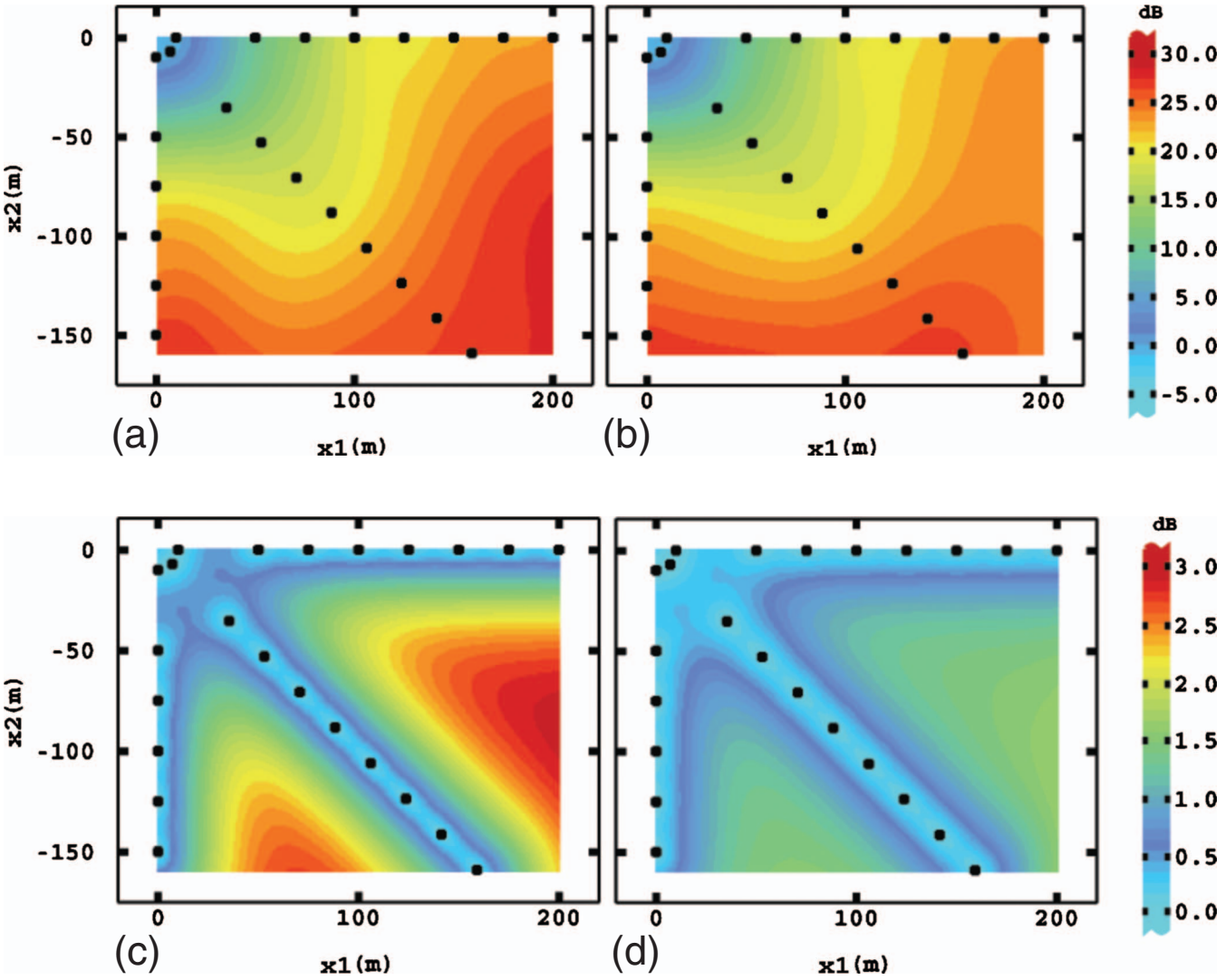

FIG. 5. Lannemezan campaign 22 June 2005 between 23:45 LST and 24:00 LST: final interpolation maps of sound attenuation (SPL rel. to ref. microphone, $L_{\mathrm{eq15\ min}}$) at 1 kHz (a) without linear drift and (b) including a linear drift; corresponding standard-deviation maps (c) without linear drift and (d) including a linear drift. Prediction height is 2 m above ground.

Hence we may rely the physical interpretation of the variogram on the physical structure of the acoustic field.

The Embleton model is not designed to follow the temporal variation in the acoustic field but provides a rough sketch of the structure of the acoustic field in our simple case study. It produces a symmetric output model (Fig. 2), whereas reality shows some anisotropy. This anisotropy was modeled through the introduction of a linear drift component in the drift model. The inclusion of the linear drift yields shorter sill and shorter range of the variogram of residuals, and lower kriging variances. A linear trend (at the scale of the data domain) is sufficient to adequately reflect the anisotropy of the acoustic field which can be observed in this case study with integrated $L_{\mathrm{eq15\ min}}$ samples. Neglecting turbulence and intermittence during the 15-min periods (first-order approximation), atmospheric effects are mainly related to vertical mean wind and vertical temperature gradients. The map of the external drift with a linear component [Fig. 3(b)] reflects this anisotropy and is close to the corresponding final kriging map [Fig. 5(b)].

In the case study (point source, flat and almost homogeneous ground), the anisotropy of the acoustic field is mostly due to wind conditions. Note that the drift is not static. Its components are estimated at each mapping time step (15 min), which allows to orientate the drift following the orientation of the wind.

Interpolation values have to be interpreted together with the corresponding standard deviation. If we assume a Gaussian distribution for the kriging error, kriging prediction values are not the reality but the most likely values of the sound field. The kriging standard deviation measures the accuracy of the kriging estimate. Thus kriging results have to be interpreted with care. When the interpolation location is far from any measurement, the uncertainty attached to the interpolated value becomes high. As an illustration, one can read the results at location $\{x_1=200, x_2=-100\}$ (following the coordinate system of the maps), where standard deviation is the highest. The interpolated value with the 95% confidence interval (twice the standard deviation) is

30.0 ± 6.0 dB without a linear drift,

24.0 ± 3.2 dB including a linear drift.

Without a linear drift, the interpolation result is too uncertain. In contrast when the linear drift is included, the confidence interval decreases by 2 and is more acceptable in that extrapolation situation.

A. Benefits from geostatistics

Through the construction of a hybrid model (a physical model included in a statistical model), geostatistics leads to interpretative maps of acoustical levels (sound attenuation from reference measurements in our case study). If a Gaussian distribution of the kriging error can be assumed, the outcome of kriging is the local conditional distribution of the acoustical level, which gives access to probability analysis (threshold level detection, for instance, confidence intervals).

Results indicate that a cubic variogram model enables a good fit of the sample variogram of the residuals for the present case study. The inclusion of the linear drift leads to low uncertainty even in extrapolation zones and improves the description of the acoustic field. This leads to an automatic mapping procedure. Input data for the whole procedure are the mean specific air flow resistivity and acoustically equivalent thickness of the ground over the whole domain of study, as well as measurements. The external drift estimation and the kriging prediction on the grid are fast to compute. As a consequence, geostatistical methods can provide real-time mapping procedures for a large band spectrum whose accuracy is given by the kriging standard-deviation map.

We applied the kriging procedure with the major assumption that the non-stationarity of the acoustical propagation can be contained in the drift only, and therefore, we further assumed that the rest (i.e., the residuals) was stationary. Stationarity of the residuals sounds peculiar and may contradict the physical intuition. However, the external drift estimation model actually does not fit better the measured values close to the source than further away, which makes our assumption reasonable in our application.

Kriging is not designed for extrapolation. Even though it is tempting to extrapolate outside the data domain, extrapolation of kriging results is not recommended. A pragmatic reason is that the statistical model, which relies on measured values, does not have information about the acoustic field apart from the data. Especially when the drift does not contain enough physical knowledge, the risk of false prediction may increase. In order to optimize the model inference, a relevant analysis of the kriging errors would require more measurement locations. Such analysis is planned in a forthcoming study.

B. Perspective of applicability

We have provided a simple physical interpretation of the interpolated values. It is much less obvious for the uncertainties. The main reason is the stationarity of residuals. We can question the fact that, from a physical perspective, mapping uncertainty may be of the same level close and further away from the source. Further validation work on that point is needed. For instance, a comparison between random perturbations of numerical prediction with a parabolic equation model and kriging uncertainty would help to envisage the issue.

More complex situations are envisaged as new case studies to test the generalization of the method. We think of varying properties of the ground (for instance, with sharp impedance jumps between the source and the measurement locations). Other existing analytical models could be introduced in the drift as an alternative to the Embleton model. Different topography and source-receiver geometry should also be studied.

We handled data sampled along three transects 45° apart, around the point source. A new modeling attempt should be carried out with sensors all around the source in order to deal with upwind and downwind conditions at the same time.

VI. CONCLUSION

Modeling sound propagation with geostatistical tools has been shown to be feasible in a simple experimental setup (omni-directional source, flat, open and almost homogeneous meadow). Thanks to the integration of an analytical model, kriging yields maps that have a sound physical interpretation. The degree of confidence of the interpolation is indicated by the kriging standard deviation; therefore, statistics in the long run become possible. However, for a clear physical interpretation of kriging uncertainty, some validation work should be pursued to compare the mapping uncertainty associated with kriging maps with that of numerical simulations from a reference model.

The method that we developed so far does not rely on meteorological measurements (the analytical model does not take micrometeorology into account). This could be seen as a conceptual drawback, but it has the practical advantage to be operational when a study must be carried out in the field in a limited time. The Embleton model is adequate for the very simple setting of the Lannemezan 2005 case study. More elaborate models might be needed as approximations of the sound field in other situations. A geostatistical application in a more complex case study of environmental acoustics is in progress. For assessing pollution from an industrial plant or from car traffic, a trade-off must be found between complexity of physical modeling and well-adapted statistical methods.

ACKNOWLEDGMENTS

The authors acknowledge The French Ministry of Ecology and Sustainable Development for its financial support to carry out the "Lannemezan 2005" experimental campaign. The authors are grateful to two anonymous reviewers and especially to Editor Kirill Horoshenkov for fruitful comments that substantially improved the content of this paper.

[1]M. E. Delany and E. N. Bazley, "Acoustical properties of fibrous absorbant materials," Appl. Acoust. **3**, 105–116 (1970).
[2]K. Attenborough, S. I. Hayek, and J. M. Lawther, "Propagation of sound over a porous half space," J. Acoust. Soc. Am. **68**, 1493–1501 (1980).

[3]T. F. W. Embleton, "Effective flow resistivity of ground surfaces determined by acoustical measurements," J. Acoust. Soc. Am. **74**, 1239–1244 (1983).
[4]V. E. Ostashev, *Acoustics in Moving Inhomogeneous Media* (E & FN Spon, London, UK, 1999).
[5]E. M. Salomons, *Computational Atmospheric Acoustics* (Kluwer, Dordrecht, The Netherlands, 2001).
[6]D. K. Wilson, J. G. Brasseur, and K. E. Gilbert, "Acoustic scattering and the spectrum of atmospheric turbulence," J. Acoust. Soc. Am. **105**, 30–34 (2007).
[7]D. Juvé, P. Blanc-Benon, and P. Chevret, "Numerical simulation of sound propagation through a turbulent atmosphere," in 5th International Symposium on Long Range Sound Propagation, Milton Keynes, UK, pp. 282–286 (1992).
[8]C. L. Pettit and D. K. Wilson, "Proper orthogonal decomposition and cluster weighted modeling for sensitivity analysis of sound propagation in the atmospheric surface layer," J. Acoust. Soc. Am. **122**, 1374–1390 (2007).
[9]D. K. Wilson, E. L. Andreas, J. W. Weatherly, C. L. Pettit, E. G. Patton, and P. P. Sullivan, "Characterization of uncertainty in outdoor sound propagation predictions," J. Acoust. Soc. Am. **121**, EL177–EL183 (2007).
[10]E. Séchet, "Modeling imprecise knowledge about the influence of meteorological conditions on sound propagation from experimental data," Ph.D. thesis, Université de Paris IX, France (1996).
[11]O. Baume, B. Gauvreau, F. Junker, H. Wackernagel, M. Bérengier, and J.-P. Chilès, "Statistical exploration of small scale variation in acoustic time series taking into account micrometeorological conditions," in Forum Acusticum, Budapest, Hungary (2005), pp. 117–122.
[12]D. G. Krige, "A statistical approach to some mine valuation and allied problems on the Witwatersrsand," MS thesis, University of Witwatersrand, South Africa (1951).
[13]G. Matheron, "Principles of geostatistics," Econ. Geol. **58**, 1246–1266 (1963).
[14]N. A. C. Cressie, "The origins of kriging," Math. Geol. **3**, 239–252 (1990).
[15]H. Wackernagel, C. Lajaunie, N. Blond, C. Roth, and R. Vautard, "Geostatistical risk mapping with chemical transport model output and ozone station data," Ecol. Modell. **179**, 177–185 (2004).
[16]J.-P. Chilès and P. Delfiner, *Geostatistics, Modeling Spatial Uncertainty*, Wiley Series on Probability and Statistics (Wiley, New-York, 1999).
[17]H. Wackernagel, *Multivariate Geostatistics*, 3rd Ed. (Springer-Verlag, Berlin, 2003).
[18]G. Hudson and H. Wackernagel, "Mapping temperature using kriging with external drift: Theory and an example from Scotland," Int. J. Climatol. **14**, 77–91 (1994).
[19]R. B. Stull, *An Introduction to Boundary Layer Meteorology* (Kluwer Academic, Dordrecht, The Netherlands, 1988).
[20]T. Foken, *Micrometeorology* (Springer-Verlag, Berlin, 2006), p. 306.
[21]F. Junker, B. Gauvreau, C. Cremezi-Charlet, and P. Blanc-Benon, "Classification of relative influence of physical parameters for long range sound propagation," in Forum Acusticum, Budapest, Hungary (2005).
[22]O. Baume, "Geostatistical approach to assess the influence of physical parameters on long range sound propagation," Ph.D. thesis, Université du Maine, France (2006).
[23]J. E. Piercy, T. F. W. Embleton, and L. C. Sutherland, "Review of noise propagation in the atmosphere," J. Acoust. Soc. Am. **61**, 1403–1418 (1977).
[24]F. Junker, C. Cremezi-Charlet, C. Gérault, B. Gauvreau, P. Blanc-Benon, B. Cotté, and D. Écotière, "Classification of relative influence of physical parameters for long range acoustic propagation experimental and numerical results," in Euronoise 2006, Tampere, Finland (2006).
[25]K. Attenborough, K. M. Li, and K. V. Horoshenkov, *Predicting Outdoor Sound* (Taylor & Francis, London, UK, 2007).